Full-State Feedback Equivalent Controller for Active Damping in LCL-Filtered Grid-Connected Inverters Using a Reduced Number of Sensors

Claudio A. Busada, Sebastian Gomez Jorge, and Jorge A. Solsona, *Senior Member, IEEE*

***Abstract*—This paper presents a method for the active damping of a grid-tie LCL inverter. This method is based solely on the feedback of the injected current into the grid and is applicable to any linear current controller. It requires a low additional computational load over that required to control a grid-tie L inverter and the same measurements. A general design methodology for the current controller, which allows positioning all of the closed-loop poles of the system at arbitrary locations (even unstable modes of the LCL filter), is proposed. Stability and robustness of the resulting system are analyzed. Simulation and experimental results that validate the proposal are presented.**

***Index Terms*—Active damping (AD), current control, grid-connected inverter, LCL filter, resonance damping.**

I. Introduction

In the grid connection of renewable resources through an inverter, using LCL filters instead of L filters is of great interest, since the latter is bulky and inefficient [1]. The LCL filter allows a large attenuation of the high frequency ripple present in the current injected to the grid, using magnetic components of lower volume than those necessary to achieve the same ripple when using an L filter. This enables compliance with the quality standards of power generation [2] at a lower cost and volume. Moreover, given an LCL filter and an L filter, both of equal magnetic circuit volume, the LCL filter allows us to meet these standards using a lower switching frequency.

Fig. 1(a) shows the connection of a three-phase inverter to the grid through an LCL filter. The presence of the filter complicates the design of the current controller, especially when this is of high order [3], because the filter has a resonance frequency. The resonance can be damped passively or actively [4]. Passive damping is the method most commonly used, although it produces additional losses and reduces the system performance [5], [6].

Manuscript received September 30, 2014; revised December 5, 2014 and February 13, 2015; accepted March 20, 2015. Date of publication April 20, 2015; date of current version September 9, 2015. This work was supported by the Universidad Nacional del Sur, CONICET, and ANPCyT, Argentina.

The authors are with the Instituto de Investigaciones en Ingeniería Eléctrica (IIIE) "Alfredo Desages" (UNS-CONICET), Departamento de Ingeniería Eléctrica y de Computadoras, Universidad Nacional del Sur (UNS), 8000 Bahía Blanca, Argentina (e-mail: cbusada@uns.edu.ar; sebastian.gomezjorge@uns.edu.ar; jsolsona@uns.edu.ar).

Digital Object Identifier 10.1109/TIE.2015.2424391

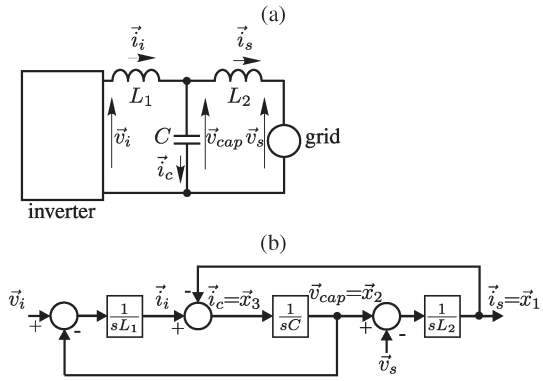

Fig. 1. (a) Grid connection through the LCL filter. (b) Plant dynamic model.

The active damping (AD) can be achieved by feeding back a signal proportional to the output current of the inverter $\vec{i}_i$ [7] or to the capacitor current $\vec{i}_c$ [8], [9]. In effect, these feedbacks emulate the presence of a virtual resistor, connected in series with L_1 or C, respectively [10], resulting in the damping of the filter. In [11], both strategies are analyzed, when a proportional-integral (PI) current controller is used. In [12], $\vec{i}_i$ and $\vec{i}_s$ are measured. The capacitor current $\vec{i}_c$, necessary to implement the feedback, is computed as the difference between the two measured currents. An equivalent method to feedback $\vec{i}_c$ is to feedback the derivative of the capacitor voltage with respect to time. While both approaches are identical in continuous time (since $d\vec{v}_{\rm cap}/dt = \vec{i}_c/C$), they differ in discrete time, and many times the damping is not possible when the resonance frequency is low [13]. The AD in [14] is achieved by adding to the voltage input to the pulsewidth modulator (PWM) the voltage $\vec{v}_{\rm cap}$ filtered by a high-pass filter. This filtering introduces the derivative action in $\vec{v}_{\rm cap}$, necessary for the feedback. The control is done on $\vec{i}_i$, and the proposal does not require additional sensors but requires estimating the voltages necessary for the controller. These voltages are estimated by assuming that the current through the capacitor is negligible at line frequency (which is not valid when the resonance frequency of the filter is low), and the estimation is dependent on the parameters of the filter. Similarly, in [15], $\vec{v}_{\rm cap}$ is filtered by a lag–lead network, introducing the derivative action. The control is done again on $\vec{i}_i$, and the strategy uses a single voltage sensor, that of $\vec{v}_{\rm cap}$, orienting the reference frame of the controller with this voltage. The phase shift between $\vec{v}_{\rm cap}$ and $\vec{v}_s$ must be compensated. This compensation is dependent on the parameters of the filter.

In most of the literature, the control is done on $\vec{i}_i$, rather than on $\vec{i}_s$. Although this allows us to take advantage of the current sensor which is normally incorporated into many commercial power inverters, AD based solely on the feedback of $\vec{i}_s$ is desirable, as shown by several papers written about it in recent times [16]–[19]. Controlling $\vec{i}_s$ instead of $\vec{i}_i$ has the advantage that both an accurate control of the power factor and the waveform of the current injected into the grid are obtained. Indeed, to achieve this accurate control when controlling $\vec{i}_i$ and $\vec{i}_s$ is not measured, it is necessary to estimate the latter. The quality of this estimate is dependent on the certainty on the parameters of the LCL filter. In [16]–[19], the control is made directly on $\vec{i}_s$, although the proposals are limited to first-order controllers [PI or proportional-resonant (PR)]. In [19], it is found that, using a discrete PR controller, it is only possible to stabilize the system by feedback of $\vec{i}_s$ when the resonance frequency of the filter is high (relatively to its proximity to the sampling frequency). When the resonance frequency of the filter is low, the additional feedback of $\vec{i}_c$ is required to achieve this (forcing us to use an additional sensor). It is also concluded that, when the filter has a specific resonant frequency (critical), not even the feedback of $\vec{i}_c$ manages to stabilize the control loop.

In [20], it is verified that the strategy of feeding back $\vec{v}_{\text{cap}}$ filtered is equivalent to filtering the total voltage input to the PWM (control action) by a linear filter network. This avoids the need to measure $\vec{v}_{\text{cap}}$, and the control can be performed through a single current sensor. In [21]–[23], this strategy is used, although the proposals are restricted again to first-order controllers (PI or PR).

All AD strategies described so far fall into what is called a partial state feedback. A description in state-space can be found in [24]. Indeed, as suggested by the block diagram of Fig. 1(b), the plant has three states: two currents $\vec{i}_s$ and $\vec{i}_c$ (or $\vec{i}_i$) and one voltage $\vec{v}_{\text{cap}}$. It is known that a partial state feedback cannot arbitrarily assign the position of all of the closed-loop poles of the system, which limits the possibilities of obtaining the desired dynamic response through this feedback strategy. In order to place the poles at arbitrary locations, it is sufficient to implement a full-state feedback [25]. This feedback requires, in principle, the addition of more sensors because, in addition to the measurement of $\vec{v}_s$ and $\vec{i}_s$, both needed to control an L filter, it is necessary to measure one more voltage and one more current [26]. These additional measurements can be avoided by using observers [27]–[29]. The estimation represents an additional computational complication, besides being dependent on the LCL filter parameters [30].

This paper proposes a new method for the AD of an LCL filter. The method can be classified among those based on the filtering of the control action [20]–[23]. However, unlike the controllers cited before, the proposal is not only applicable to first-order controllers. The characteristics of the method proposed here are the following.

1) The AD is achieved through the feedback of a single signal, the injected grid current $\vec{i}_s$. Effective closed-loop control of this current is assured.
2) It enables full control of the dynamics of the closed-loop system, enabling arbitrary placing of all of the closed-loop poles. This feature ensures the AD of the LCL filter, moving the unstable poles to stable positions.
3) The proposal is not limited to first-order controllers but is applicable to any linear current controller.
4) It is applicable regardless of the position of the resonance frequency of the filter within the control band.
5) The additional computational load required with respect to that necessary to control an L filter is low.

The proposed AD method is formulated in both continuous and discrete time. As an application example, it is used to control an LCL filter through a typical high-order current controller. Additionally, the robustness of the closed-loop system is analyzed. Both simulation and experimental results are presented to validate the proposal.

II. LCL Filter Model

Fig. 1 shows the variables that will be used to model the plant. In what follows, a complex space vector notation is used to represent a three-phase system [31], although the proposal is also applicable to single-phase systems. The input $\vec{v}_s$ is an external disturbance to the system and does not affect its stability. In what follows, it will be assumed, without loss of generality, that $\vec{v}_s = 0$. The plant consists of three states. Using as state variables the signals $\vec{i}_s \equiv \vec{x}_1, \vec{v}_{\text{cap}} \equiv \vec{x}_2$, and $\vec{i}_c \equiv \vec{x}_3$ and assuming that $\vec{v}_s = 0$, the plant model is

$$\dot{\mathbf{x}} = \mathbf{A}\mathbf{x} + \mathbf{B}\vec{v}_i \tag{1}$$

$$\vec{i}_s = \mathbf{C}\mathbf{x} \tag{2}$$

where $\mathbf{x} = [\vec{x}_1 \ \ \vec{x}_2 \ \ \vec{x}_3]^T, \mathbf{B} = [0 \ \ 0 \ \ 1/L_1]^T, \mathbf{C} = [1 \ \ 0 \ \ 0]$, and

$$\mathbf{A} = \begin{bmatrix} 0 & \frac{1}{L_2} & 0 \\ 0 & 0 & \frac{1}{C} \\ 0 & -\frac{1}{L_p} & 0 \end{bmatrix} \tag{3}$$

with $L_p = L_1 L_2/(L_1 + L_2)$. The plant (1) is a third-order system. The characteristic polynomial of $\mathbf{A}$ is $\lambda(\lambda^2 + \omega_o^2)$, with $\omega_o = \sqrt{1/(L_p C)}$. The eigenvalues of $\mathbf{A}$ are $\lambda_1 = 0$ and $\lambda_{2,3} = \pm j\omega_o$. The plant is thus unstable and has a resonance at frequency ω_o.

The proportional feedback of $\vec{i}_c$ to the input $\vec{v}_i$ shifts the eigenvalues $\lambda_{2,3}$ to stable positions. Indeed, imposing $\vec{v}_i = [0 \ \ 0 \ \ -K_d]\mathbf{x}$ in (1), the closed-loop characteristic polynomial results to $\lambda(\lambda^2 + 2\zeta\omega_o\lambda + \omega_o^2)$, where $\zeta = K_d/(2L_1\omega_o)$ represents the damping achieved through feedback. For the underdamped system, $\lambda_{2,3} = \omega_o[-\zeta \pm j\sqrt{(1-\zeta^2)}]$. Both eigenvalues are stable for $\zeta > 0$, and $|\lambda_{2,3}| = \omega_o$ for any $\zeta < 1$. This means that the proportional feedback of $\vec{i}_c$ allows adding damping to the filter. However, this does not allow us to arbitrarily assign the position of the poles of the closed-loop system because, with this feedback, it still is $\lambda_1 = 0$ and $\lambda_{2,3}$ cannot be arbitrarily placed. Through a similar procedure, it can be verified that the proportional negative feedback of $\vec{i}_s$ or $\vec{v}_{\text{cap}}$ does not stabilize the system either. On the other hand, the feedback of $\vec{i}_i$ does, since this signal includes the feedback

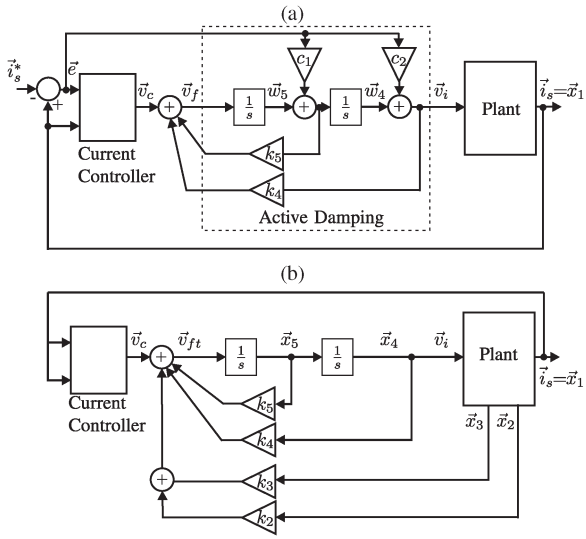

Fig. 2. Proposed AD strategy (continuous-time case). (a) Proposal implementation. (b) Transformed system used to compute the feedback gains.

of $\vec{i}_c$: $\vec{i}_i = \vec{i}_c + \vec{i}_s$. This partly explains why, in most of the applications found in the literature, it is preferred to perform the closed-loop control of $\vec{i}_i$ instead of $\vec{i}_s$.

III. Proposed AD

To ensure the stability of the system, it is necessary to relocate all of the closed-loop poles at stable positions. A full-state feedback enables the arbitrary pole assignment but requires additional measurements. In what follows, a new strategy which does not require these additional measurements is proposed. Fig. 2(a) shows a block diagram summarizing the proposal. In this diagram, $\vec{i}_s^*$ represents the reference output current which must be tracked by $\vec{i}_s$, and the block "Current Controller" represents any linear current controller that provides an output signal $\vec{v}_c$ resulting, for the condition $\vec{i}_s^* = 0$, from a linear combination of all of its states and $\vec{x}_1$

$$\vec{v}_c = k_1\vec{x}_1 + \sum_{n=6}^{N} k_n\vec{x}_n \tag{4}$$

where it is assumed that $\vec{x}_6$, $\vec{x}_7, \ldots,$ $\vec{x}_N$ are the internal states of the controller and $k_n, n = 1, 6, \ldots, N$, are the feedback gains. Proportional controllers (with only $k_1 \neq 0$) or PI controllers ($N = 6$) are the simplest controllers that fall within this category. The block "Active Damping" in Fig. 2(a) represents the linear filter proposed in this paper to arbitrarily assign the poles of the closed-loop system. Note that this block requires only information about the error $\vec{i}_s - \vec{i}_s^*$ and about $\vec{v}_c$ (the output of the current controller), showing that the proposed AD strategy can be implemented using the same number of sensors required to control a grid-tie L inverter. The block is located at the input of the plant (1) and involves two new states: $\vec{w}_4$ and $\vec{w}_5$. Hereinafter, as the stability of the system is analyzed, it is assumed that $\vec{i}_s^* = 0$, since this input does not affect the stability of the system. The equations describing the block "Active Damping" in Fig. 2(a), with $\vec{i}_s^* = 0$, are as follows:

$$\dot{\vec{w}}_4 = \vec{w}_5 + c_1\vec{x}_1 \tag{5}$$
$$\dot{\vec{w}}_5 = \vec{v}_c + k_5\vec{w}_5 + k_4\vec{w}_4 + (c_1k_5 + c_2k_4)\vec{x}_1 \tag{6}$$
$$\vec{v}_i = \vec{w}_4 + c_2\vec{x}_1. \tag{7}$$

Note in Fig. 2(a) that the internal states of the block "Active Damping" are fed back to the input $\vec{v}_f$ of the block. This, together with (4), shows that $\vec{v}_f$ is a linear combination of all of the states of the system, except for the two states of the plant that are not measured, $\vec{x}_2$ and $\vec{x}_3$. Despite the lack of contribution of these two states in $\vec{v}_f$, the block "Active Damping" allows us to arbitrarily reassign the position of all of the poles of the closed-loop system.

Proposition 1: If the constants c_1 and c_2 of the block "Active Damping" in Fig. 2(a) are chosen as follows:

$$c_1 = k_2L_2 + k_5k_3L_2C \tag{8}$$
$$c_2 = k_3L_2C \tag{9}$$

with k_2 and k_3 arbitrary constants, then the block "Active Damping" (5)–(7) allows us to arbitrarily place all of the poles of the closed-loop continuous system.

Proof: Define the following linear transformation for the state variables of the block "Active Damping" in Fig. 2(a)

$$\vec{x}_4 = \vec{w}_4 + c_2\vec{x}_1 \tag{10}$$
$$\vec{x}_5 = \vec{w}_5 + c_1\vec{x}_1 + \frac{c_2}{L_2}\vec{x}_2. \tag{11}$$

Now, using (10) and (11) in (5)–(7), together with (1), (8), and (9), the equations that describe the block "Active Damping", in terms of the new states $\vec{x}_4$ and $\vec{x}_5$, are

$$\dot{\vec{x}}_4 = \vec{x}_5 \tag{12}$$
$$\dot{\vec{x}}_5 = \vec{v}_c + k_5\vec{x}_5 + k_4\vec{x}_4 + k_3\vec{x}_3 + k_2\vec{x}_2 = \vec{v}_{ft} \tag{13}$$
$$\vec{v}_i = \vec{x}_4. \tag{14}$$

Fig. 2(b) shows the transformed system, with $\vec{i}_s^* = 0$. Note that, replacing (4) in (13), it is verified that the input $\vec{v}_{ft}$ of the transformed system is a linear combination of all of its states, even those of the plant that are not measured, $\vec{x}_2$ and $\vec{x}_3$

$$\vec{v}_{ft} = \sum_{n=1}^{N} k_n\vec{x}_n. \tag{15}$$

Given this state feedback, if the open-loop system is controllable, it is known that the constants $k_n, n = 1, \ldots, N$, in (15) allow us to arbitrarily assign the location of all of the poles of the closed-loop system of Fig. 2(b) [32]. As this transformed system is related with the one in Fig. 2(a) through a similarity transformation (the linear transformation of states (10) and (11)), provided that c_1 and c_2 satisfy (8) and (9), it results that both systems will have the same pole locations. Then, the choice (8) and (9) allows us to arbitrarily place all of the poles of the closed-loop continuous system of Fig. 2(a). □

The strategy to follow in designing a current controller is therefore simple. First, obtain the gains $\vec{k}_n, n = 1, \ldots, N$, that achieve the desired relocation of all poles of the transformed

system of Fig. 2(b) (which assumes that the unmeasured signals $\vec{x}_2$ and $\vec{x}_3$ are available). Then, (8) and (9) are used to compute the gains c_1 and c_2 needed to implement, along with k_4 and k_5, the block "Active Damping" in Fig. 2(a), which does not require the unmeasured signals. The remaining gains $k_n, n = 1, 6, \ldots, N$, are used to implement the block "Current Controller" in Fig. 2(a).

IV. Discrete-time Design

In a digital implementation, the k_i gains can be calculated in the continuous-time domain and then proceed to the discretization of the controller. Another strategy is to describe the plant in the discrete-time domain and calculate the k_i gains in such domain. In general, this latter approach is better, especially when dealing with high-order controllers, where the phase introduced by the sampling process and the processing delay can destabilize a design that is stable in the continuous-time domain [13]. In what follows, the proposed AD strategy is formulated in the discrete-time domain, so that the controller can be designed directly on it.

In terms of transfer function, the plant (1)–(3) is described by

$$H(s) \equiv \frac{\vec{I}_s(s)}{\vec{V}_i(s)} = \frac{\omega_o^2/L_T}{s\left(s^2+\omega_o^2\right)} \tag{16}$$

where $L_T = L_1 + L_2$ and $\vec{I}_s(s)$ and $\vec{V}_i(s)$ represent the Laplace transforms of $\vec{i}_s$ and $\vec{v}_i$, respectively. Applying the zero-order hold (ZOH) discretization with sampling time T_s to $H(s)$, the discrete transfer function results to

$$H(z) \equiv \frac{\vec{I}_s(z)}{\vec{V}_i(z)} = \frac{b_1 z^{-1} + b_2 z^{-2} + b_3 z^{-3}}{1 + a_1 z^{-1} + a_2 z^{-2} + a_3 z^{-3}} \tag{17}$$

where b_i and $a_i, i = 1, 2, \text{or } 3$, are real constants. In the discrete case, the processing delay must be included in the system model. It will be represented here as a delay located at the input of (17). In state variables, this delay adds an additional state $\vec{x}_d$ to the system model. Representing (17) in its observable canonical form [32] and incorporating this additional state, a plant representation is

$$\mathbf{x}(k+1) = \mathbf{A_d}\mathbf{x}(k) + \mathbf{B_d}\vec{v}_i(k) \tag{18}$$

$$\vec{i}_s(k) = \mathbf{C_d}\mathbf{x}(k) \tag{19}$$

where $\mathbf{x} = [\vec{x}_1 \quad \vec{x}_2 \quad \vec{x}_3 \quad \vec{x}_d]^T, \mathbf{B_d} = [0 \quad 0 \quad 0 \quad 1]^T, \mathbf{C_d} = [1 \ 0 \ 0 \ 0]$

$$\mathbf{A}_d = \begin{bmatrix} -a_1 & 1 & 0 & b_1 \\ -a_2 & 0 & 1 & b_2 \\ -a_3 & 0 & 0 & b_3 \\ 0 & 0 & 0 & 0 \end{bmatrix} \tag{20}$$

$\vec{x}_1 = \vec{i}_s$, and $\vec{x}_2$ and $\vec{x}_3$ are unmeasured states (unlike the continuous case, in the discrete case is $\vec{x}_2 \neq \vec{v}_{\text{cap}}$ and $\vec{x}_3 \neq \vec{i}_c$). The discrete-time version of the block "Active Damping" is shown in Fig. 3(a) (where q^{-1} represents the unit delay operator). The block contains three states, one more than in the continuous case. This increase in the number of states is consistent with the increase in the order of the plant introduced by the additional state $\vec{x}_d$. Note in Fig. 3(a) that the state $\hat{\vec{x}}_d$ in the block "Active Damping" is the estimation of $\vec{x}_d$, which is obtained by delaying the signal $\vec{v}_i$ one sample. The equations describing the block "Active Damping" are the following (with $\vec{i}_s^* = 0$):

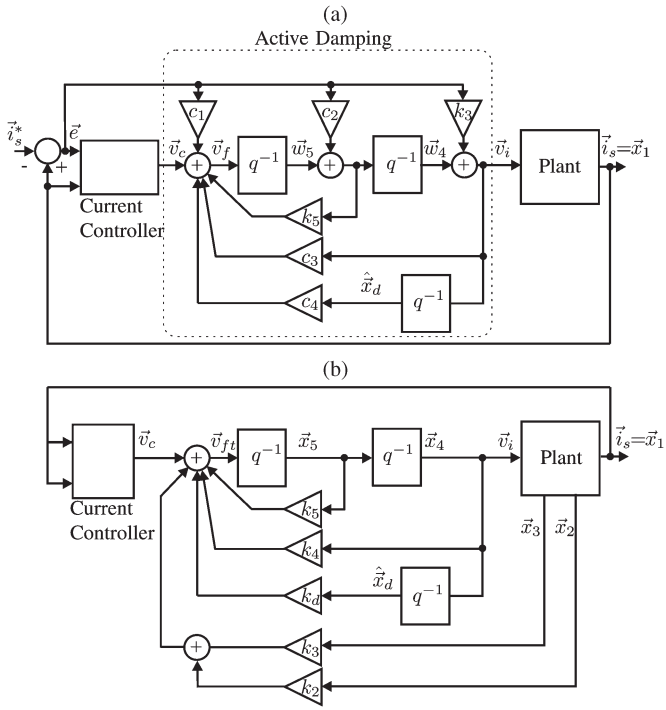

Fig. 3. Proposed AD strategy (discrete-time case). (a) Proposal implementation. (b) Transformed system used to compute the feedback gains.

$$\vec{w}_4(k+1) = \vec{w}_5(k) + c_2\vec{x}_1(k) \tag{21}$$

$$\vec{w}_5(k+1) = \vec{v}_c + c_4\hat{\vec{x}}_d(k) + k_5\vec{w}_5(k) + c_3\vec{w}_4(k) + k_T\vec{x}_1(k) \tag{22}$$

$$\hat{\vec{x}}_d(k+1) = \vec{w}_4(k) + k_3\vec{x}_1(k) \tag{23}$$

$$\vec{v}_i(k) = \vec{w}_4(k) + k_3\vec{x}_1(k) \tag{24}$$

where $k_T = c_1 + c_2k_5 + c_3k_3$.

Proposition 2: If the constants $c_1 - c_4$ of the block "Active Damping" in Fig. 3(a) are chosen as follows:

$$c_1 = k_2a_1 + k_3a_2 \tag{25}$$

$$c_2 = k_3a_1 + k_2 + k_3k_5 \tag{26}$$

$$c_3 = k_4 - k_3b_1 \tag{27}$$

$$c_4 = -k_3b_2 - k_2b_1 + k_d \tag{28}$$

with k_2 and k_4 arbitrary constants, then the block "Active Damping" (21)–(24) allows us to arbitrarily place all of the poles of the closed-loop discrete system.

Proof: Define the following linear transformation for the state variables of the block "Active Damping" in Fig. 3(a)

$$\vec{x}_4 = \vec{w}_4 + k_3\vec{x}_1 \tag{29}$$

$$\vec{x}_5 = \vec{w}_5 + (c_2 - k_3a_1)\vec{x}_1 + k_3b_1\hat{\vec{x}}_d + k_3\vec{x}_2. \tag{30}$$

Now, using (29) and (30) in (21)–(24), together with (18) and (25)–(28), the equations that describe the block "Active Damping," in terms of the new states $\vec{x}_4$ and $\vec{x}_5$, are

$$\vec{x}_4(k+1) = \vec{x}_5(k) \tag{31}$$

$$\vec{x}_5(k+1) = \vec{v}_c + k_d\hat{\vec{x}}_d + \sum_{n=2}^{5} k_n\vec{x}_n = \vec{v}_{ft} \tag{32}$$

$$\hat{\vec{x}}_d(k+1) = \vec{x}_4(k) \tag{33}$$

$$\vec{v}_i = \vec{x}_4(k). \tag{34}$$

Fig. 3(b) shows the transformed system, with $\vec{i}_s^* = 0$. Note that, if in (32) $\vec{v}_c$ is a signal of the form of (4) and if $\hat{\vec{x}}_d = \vec{x}_d$ (which implies assuming an inverter free of distortion), then $\vec{v}_{ft}$ results to a linear combination of all of the states of the system, even those not measured

$$\vec{v}_{ft} = k_d\hat{\vec{x}}_d + \sum_{n=1}^{N} k_n\vec{x}_n. \tag{35}$$

This input allows us to arbitrarily place all of the closed-loop poles of the transformed system of Fig. 3(b). As this transformed system is related with the one in Fig. 3(a) through a similarity transformation [the linear transformation of states (29) and (30), provided that $c_1 - c_4$ satisfy (25)–(28)], it results that both systems will have the same pole locations. Then, the choice (25)–(28) allows us to arbitrarily place all of the poles of the closed-loop discrete system of Fig. 3(a). □

The strategy to place these poles consists in calculating the gains $k_n, n = 1, \ldots, N$, and k_d that place the closed-loop poles of the transformed system in Fig. 3(b) at the desired locations and then use (25)–(28) to compute the gains $c_1 - c_4$ needed to implement, along with k_3 and k_5, the block "Active Damping" in Fig. 3(a). The remaining gains $k_n, n = 1, 6, \ldots, N$, are used to implement the block "Current Controller" in Fig. 3(a).

V. Current Controller With AD

As an example, in what follows of this paper, the AD method described in the previous section will be used together with a typical high-order linear current controller. The LCL filter that will be used has the following parameters: $L_1 = 1.5$ mH, $L_2 = 2.28$ mH, and $C = 9.88$ μF (resonance frequency at 1683 Hz). The sampling frequency and PWM frequency will be 5 kHz ($T_s = 200$ μs). The structure proposed in [33] was used here for the current controller. In this controller, the reference current $\vec{i}_s^*$ is obtained by scaling the measured grid voltage $\vec{v}_s$, and at steady state, $\vec{i}_s$ results in phase with the fundamental component of $\vec{v}_s$. The controller is based on resonant filters tuned to specific frequencies and

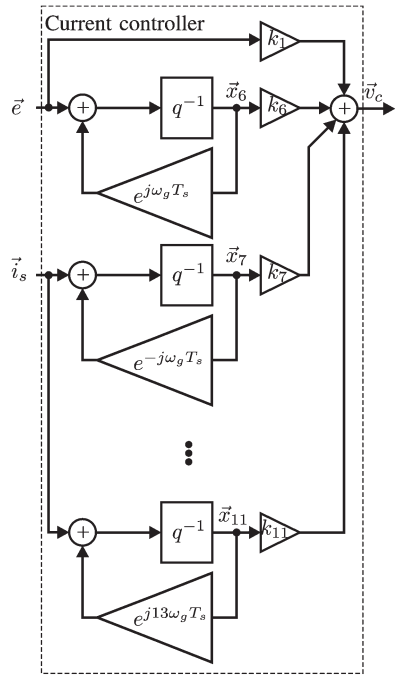

Fig. 4. Current controller block diagram.

harmonic sequences. These filters are known as reduced-order generalized integrators (ROGIs). For the designed controller, ROGIs tuned at $+1, -1, -5, +7, -11$, and $+13$ times ω_g (the fundamental angular frequency of the grid voltage) were used. A block diagram of this controller is shown in Fig. 4. To design the controller, from Fig. 3(b) and (18)–(20) and forcing all gains to zero in Fig. 4, a new system state vector is defined $\mathbf{x}_c = [\vec{x}_1\ \vec{x}_2\ \vec{x}_3\ \vec{x}_d\ \vec{x}_4\ \vec{x}_5\ \vec{x}_6\ \vec{x}_7, \ldots, \vec{x}_{11}]^T$, where $\vec{x}_k$, with $k = 6, 7, \ldots, 11$, are the states of the ROGIs. With this new state vector and taking $\vec{v}_{ft}$ as the input to the system, the state variable description of the open-loop discrete-time transformed system of Fig. 3(b) is shown in (36), shown at the bottom of the next page. In this equation, $0_{i\times k}$ is the $i \times k$ zero matrix. By imposing the full state feedback $\vec{v}_{ft} = \mathbf{K}\vec{x}_c$ in (36), with $\mathbf{K} = [k_1, k_2, k_3, k_d, k_4, k_5, k_6, k_7, \ldots, k_{11}]$, the transition matrix of the closed-loop systems results to $\mathbf{A_{cl}} = \mathbf{A_c} + \mathbf{B_c}\mathbf{K}$. The gain vector $\mathbf{K}$ can now be chosen through any method that allows arbitrary assignation of the closed-loop poles (e.g., through the Ackerman's formula or the linear quadratic regulator (LQR) theory; see [34]). Once the vector $\mathbf{K}$ is known, the gains $c_1 - c_4$ are computed by using (25)–(28). The system (36) has 12 complex states. The presence of complex coefficients in $\mathbf{A_c}$ means that α and β axes are coupled. This means that the actual system has 24 coupled real discrete states which must be controlled. The complexity of this system is the reason why the LQR method was chosen to find the gain vector $\mathbf{K}$.

This strategy frees the designer from choosing the pole locations and, in general, results in a robust closed-loop system. In the LQR theory, $\mathbf{K}$ must be chosen to minimize the cost function

$$J = \sum_{k=0}^{\infty} \mathbf{x_c}^*(k)\mathbf{Q}\mathbf{x_c}(k) + R\ |\vec{v}_{ft}(k)|^2 \tag{37}$$

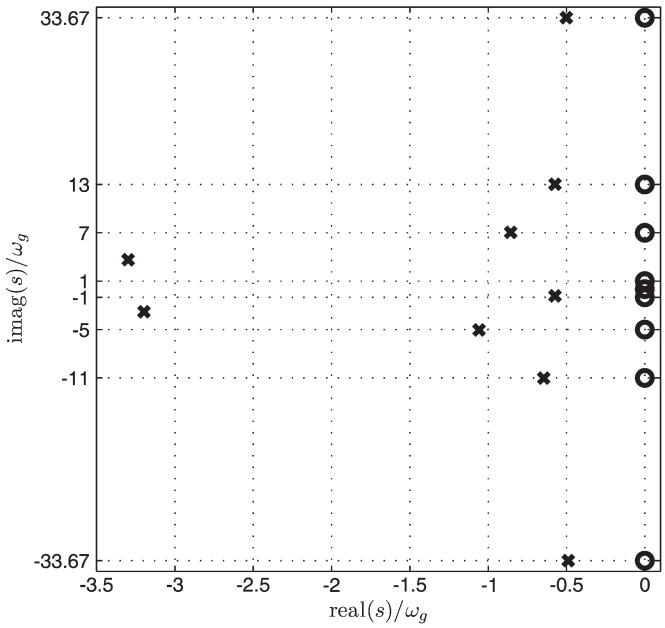

Fig. 5. Dominant poles place for the open-loop system (o) and for the closed-loop system (x).

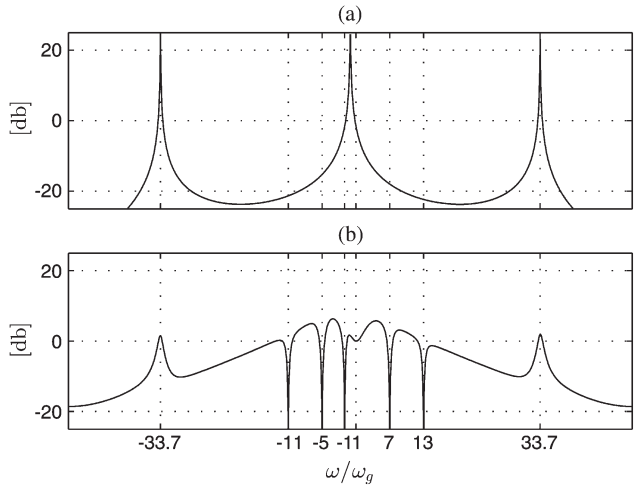

Fig. 6. (a) Frequency response (modulus) of the open-loop LCL filter transfer function $\vec{I}_s(s)/\vec{V}_i(s)$. (b) Frequency response (modulus) of the closed-loop transfer function $\vec{I}_s(z)/\vec{I}_s(z)^*$.

where $*$ denotes transpose conjugate, $\mathbf{Q} \in \mathbb{C}^{(2+r)\times(2+r)}$ is a Hermitian matrix, and $R \in \mathbb{R}$. The elements of $\mathbf{Q}$ and R are weighting factors. Given $\mathbf{Q}$ and R, the gain vector $\mathbf{K}$ that minimizes (37) can be found in practice using the MATLAB function $\texttt{dlqr}(\mathbf{A_c}, \mathbf{B_c}, \mathbf{Q}, R)$. The elements of $\mathbf{Q}$ (generally a diagonal matrix) and R are chosen empirically, verifying that the time response is satisfactory and that the closed-loop system is robust (verifying the stability of $\mathbf{A_{cl}} = \mathbf{A_c} + \mathbf{B_c}\mathbf{K}$ to bounded variations of the parameters of the plant). In [26], the guidelines for the selection of $\mathbf{Q}$ and R are given. For the implemented system, the following values were used: $\mathbf{Q} = \text{diag}([1\ 1\ 1\ 1\ 1\ 1\ 10\ 1\ 1\ 1\ 1\ 1])$ and $R = 1$.

For the designed controller, Fig. 5 shows the geometric place of the dominant poles of the continuous-time system (which is more illustrative than its discrete-time system counterpart). The plane was normalized to ω_g. To craft this figure, the dominant poles z_p of the discrete system have been mapped to continuous time through the transformation $s = \ln(z_p)/T_s$. The nine dominant poles of the open-loop system of Fig. 3(b) are shown with circles: three poles from the LCL filter (0 and $\pm j33.67$), along with those of the ROGIs tuned at harmonic frequencies $+1, -1, -5, +7, -11$, and $+13$ times ω_g. The locations of the nine dominant poles of the closed-loop system are shown with crosses. These poles, as expected, are located at stable positions. The remaining closed-loop poles not shown (not dominant) are located at $-182.9 - j18.72$, $-182.9 + j14.62$ y $-182.9 + j47.95$ (normalized with respect to ω_g), far from the imaginary axis. Note that properly choosing $\mathbf{K}$ so that $\mathbf{A_{cl}} = \mathbf{A_c} + \mathbf{B_c}\mathbf{K}$ is stable shifts the unstable LCL filter poles to stable locations, verifying the AD capabilities of the proposed method.

Fig. 6(a) shows the modulus of the frequency response of the open-loop LCL filter transfer function $\vec{I}_s(s)/\vec{V}_i(s)$, defined in (16). The response to positive frequencies is the response to a positive sequence input vector $\vec{v}_i$, and the response to negative frequencies is the response to a negative sequence one [33]. The resonance of the LCL filter is located at 33.7 ω_g (1683 Hz for a 50-Hz grid). For the designed controller, Fig. 6(b) shows the modulus of the frequency response of the closed-loop transfer function $\vec{I}_s(z)/\vec{I}_s^*(z)$ (obtained by evaluating this transfer function at $z = e^{j\omega T_s}$), where $\vec{I}_s(z)$ and $\vec{I}_s^*(z)$ are the z transforms of the ZOH discretizations of $\vec{i}_s$ and $\vec{i}_s^*$, respectively. As can be seen in Fig. 6(b), the infinite gain peaks at the resonance frequency of the LCL filter shown in Fig. 6(a) have here a finite magnitude, consistently with the closed-loop pole location shift to stable positions showed in Fig. 5.

$$\begin{bmatrix} \mathbf{x} \\ \vec{x}_4 \\ \vec{x}_5 \\ \vec{x}_6 \\ \vec{x}_7 \\ . \\ . \\ \vec{x}_{11} \end{bmatrix}(k+1) = \underbrace{\left[\begin{array}{cccc|c|cccccc} & \mathbf{A_d} & & & \mathbf{B_d} & & & 0_{4\times7} & & & \\ 0 & 0 & 0 & 0 & 0 & 1 & 0 & 0 & 0 & . & . & 0 \\ 0 & 0 & 0 & 0 & 0 & 0 & 0 & 0 & 0 & . & . & 0 \\ 1 & 0 & 0 & 0 & 0 & 0 & 0 & e^{j\omega_g T_s} & 0 & . & . & 0 \\ 1 & 0 & 0 & 0 & 0 & 0 & 0 & 0 & e^{-j\omega_g T_s} & . & . & 0 \\ . & . & . & . & . & . & . & . & . & . & . & \\ . & . & . & . & . & . & . & . & . & . & . & \\ 1 & 0 & 0 & 0 & 0 & 0 & 0 & 0 & 0 & . & . & e^{j13\omega_g T_s} \end{array}\right]}_{\mathbf{A_c}} \underbrace{\begin{bmatrix} \mathbf{x} \\ \vec{x}_4 \\ \vec{x}_5 \\ \vec{x}_6 \\ \vec{x}_7 \\ . \\ . \\ \vec{x}_{11} \end{bmatrix}}_{\mathbf{x}_c}(k) + \underbrace{\begin{bmatrix} 0_{4\times1} \\ 0 \\ 1 \\ 0 \\ 0 \\ . \\ . \\ 0 \end{bmatrix}}_{\mathbf{B_c}} \vec{v}_{ft}(k) \quad (36)$$

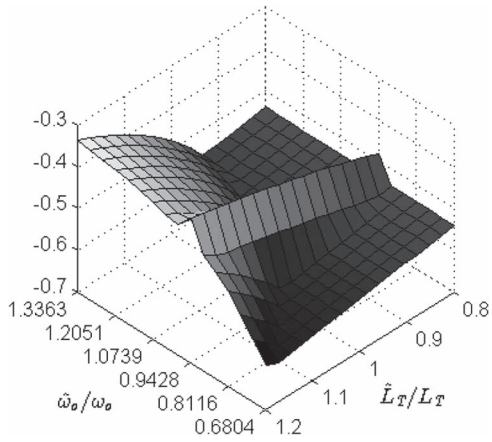

Fig. 7. Normalized largest modulus of the closed-loop eigenvalues to a parametric variation of $\pm 20\%$ in L_1 and L_2 and $-30/+80\%$ in C.

The designer has control over the location of the closed-loop poles by choosing $\mathbf{K}$ but has no control over the location of the closed-loop zeros. The locations of these zeros match the locations of the controller poles at harmonic frequencies $-1, -5, +7, -11$, and $+13$ times ω_g. Fig. 6(b) clearly shows the location of these zeros.

VI. Robustness To Parametric Variation

An analysis of the robustness to parametric variations of the closed-loop system designed in the previous section will be performed. The varying parameters will be L_1, L_2, and C. Note that the variation in L_2 includes the case where the variation occurs in the grid impedance. To perform the analysis, the gains of the current controller are first computed using the nominal values of the LCL filter parameters. Then, each parameter of the LCL filter is varied within a bounded set. For each set of parameters, the eigenvalues of the closed-loop state matrix of the discrete system are computed. The stability on each set will be guaranteed, if the modulus of all eigenvalues is less than unity. Note that, even though the LCL filter has three parameters, namely, L_1, L_2, and C, its transfer function (16) is characterized through only two parameters: L_T and ω_o. For L_1, L_2, and C varying within the bounded sets: $C_{\min} \leq C \leq C_{\max}, L_{1\min} \leq L_1 \leq L_{1\max}$, and $L_{2\min} \leq L_2 \leq L_{2\max}$, the variation of L_T and ω_o results in the bounded sets

$$L_{1\min} + L_{2\min} \leq L_T \leq L_{1\max} + L_{2\max}$$

$$\sqrt{\frac{L_{1\max} + L_{2\max}}{L_{1\max} L_{2\max} C_{\max}}} \leq \omega_o \leq \sqrt{\frac{L_{1\min} + L_{2\min}}{L_{1\min} L_{2\min} C_{\min}}}.$$

Fig. 7 shows the maximum real part of the eigenvalues of the closed-loop discrete system transformed to the complex plane through $s = \ln(z_p)/T_s$ (normalized to ω_g), for a parametric variation of $\pm 20\%$ in L_1 and L_2 and $-30/+80\%$ in C, which translates to a variation of $\pm 20\%$ in L_T and of $+33\%/-32\%$ in ω_o. As can be seen, for this variation, the eigenvalues are always within the negative real axis, which guarantees the stability of the system under study to a typical variation in the parameters of the filter.

VII. Simulation and Experimental Results

For the controller designed in Section V, simulation results are shown, along with the experimental results obtained from a prototype implemented to this end. The three-phase inverter was built using IGBT IRG4PH50UD. The dead time used for the inverter switches was 1 μs, which was included in the simulation. Also, the switch conduction voltage drops were here modeled through a constant voltage source of 2.5 V, in series with a resistance $R_{\text{on}} = 1$ mΩ. The controller was implemented in a fixed-point digital signal processor TMS320F2812, with a clock frequency of 150 MHz. The effects of quantization of the fixed point were included in the simulation. The sampling frequency and the PWM frequency were 5 kHz. The measurements necessary for the control (phase currents and voltages) were filtered with a first-order antialias filter with a cutoff frequency of 2340 Hz. This filter was also modeled in the simulations. The internal resistances of the inductances L_1 and L_2 were also included, and their values were 143 and 303 mΩ, respectively. The dc bus voltage of the converter was set to 400 Vdc, the grid voltage was 110 Vrms, 50 Hz, and the nominal power of the converter was 2 kVA (which implies that $L_1 = 0.026$ pu, $L_2 = 0.039$ pu, and $C = 17.5$ pu).

For the purposes of comparison, the grid voltage captured during the experimental results was used as the grid voltage in the simulations. Also, the startup times of the controller were tuned for the simulation, in order to match those observed in the experimental results.

Fig. 8 shows the simulation and experimental results at startup, when the reference current $\vec{i}_s^*$ is set to inject 5 Arms to the grid. In this figure, the voltage of the phase a (v_s^a) of the grid is shown along with the three-phase injected currents $(i_s^a, i_s^b$, and $i_s^c)$. The initial current observed before the converter startup is the current drained from the grid by the series circuit composed of L_2 and C, which is initially connected to the grid. It can be seen both in the simulation and experimental results that the startup of the controller is soft and that it converges in approximately one grid cycle.

Fig. 9 shows the simulation and experimental results of the converter once steady state is reached. In this figure, the following magnitudes of phase a are shown: the grid voltage (v_s^a), the capacitor voltage (v_{cap}^a), the inverter output current (i_i^a), and the current injected to the grid (i_s^a). The attenuation produced by the LCL filter on the high-frequency harmonic content present in i_i^a can clearly be noted by comparing i_s^a with i_i^a. The low cutoff frequency of the LCL filter (1683 Hz) allows us to use a low PWM frequency (5 kHz) and still achieve a low harmonic content in i_s^a. The total harmonic distortion (THD) of current i_s^a shown in Fig. 9(b) was THD $= 1.77\%$, whereas the voltage v_s^a had a distortion of THD $= 2.53\%$.

Fig. 10 shows the transient of the injected current to a step in the reference current from 5 to 2.5 Arms. The signals shown in this figure are the same as those shown in Fig. 8. It can be seen that the transient response of the system is as expected, with the currents converging without excessive overshoot in one grid cycle.

The matching between the measured and simulated responses shown in Figs. 8–10 leads us to conclude that a good

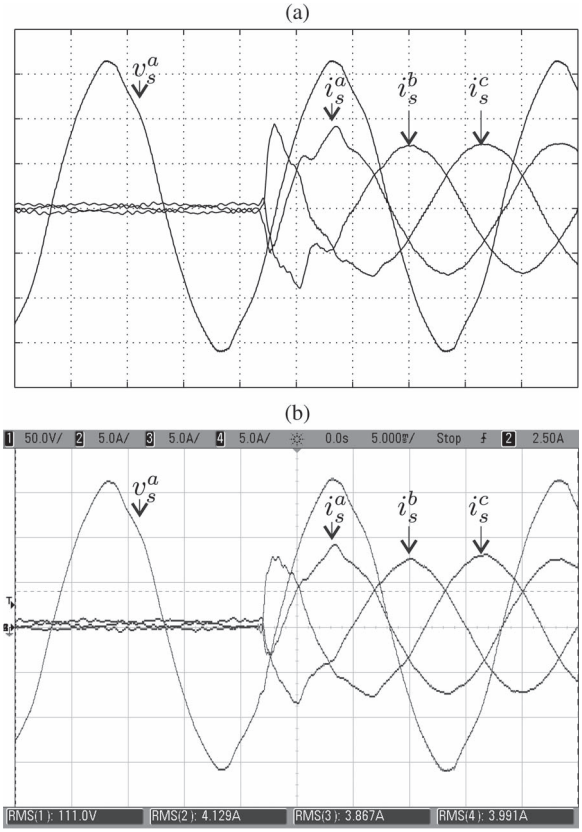

Fig. 8. Converter startup. Voltage scale: 50 V/div, current scale: 5 A/div, time scale: 5 ms/div. (a) Simulation. (b) Experimental.

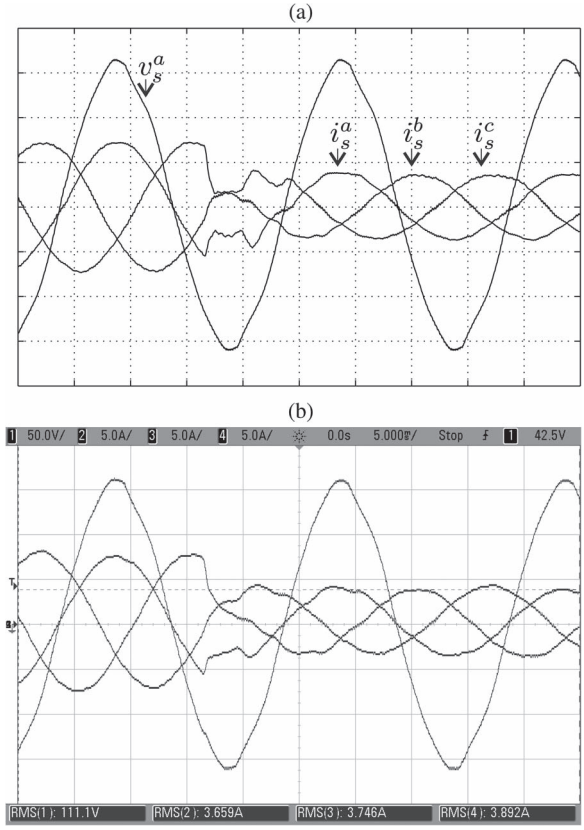

Fig. 10. Current gain step. Voltage scale: 50/div, current scale: 5 A/div, time scale: 5 ms/div. (a) Simulation. (b) Experimental.

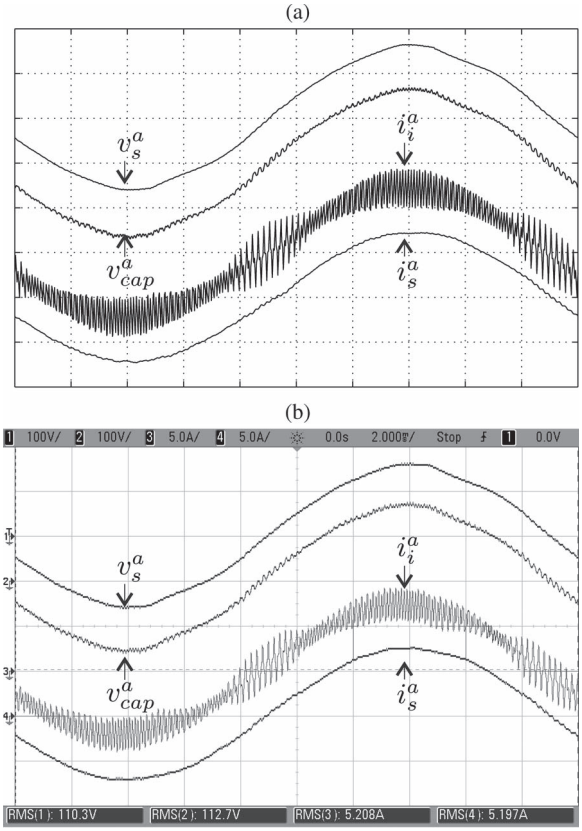

Fig. 9. Steady state. Voltage scale: 100 V/div, current scale: 5 A/div, time scale: 2 ms/div. (a) Simulation. (b) Experimental.

simulation model is available. This model will be used to predict the behavior of the system under different conditions than those implemented experimentally. First, to verify the robustness of the designed controller to parametric uncertainties, the values of L_1, L_2, and C will be increased by $+20\%$, $+20\%$, and $+80\%$, respectively (the maximum parametric mistuning which was used to compute Fig. 7). With these new parameters, the resonance frequency of the LCL filter is 0.684 times lower than its nominal value (it goes from 1683 to 1145 Hz), resulting to $\pm 22.9\ \omega_g$. This new resonance frequency is located only 1.7 times above $+13\omega_g$, the maximum frequency that the controller compensates.

Fig. 11(a) shows the startup time response of the closed-loop system operating with the mistuned plant. Note that the time response is very similar to that of Fig. 8, even though the parameters of the LCL filter are widely mistuned. This leads us to conclude that not only the controller is stable to a wide parametric variation but also that the dynamic response of the system is almost the same as with nominal parameters. For comparison purposes, Fig. 11(b) shows the modulus of the frequency response of the open-loop LCL filter transfer function $\vec{I}_s(s)/\vec{V}_i(s)$, and Fig. 11(c) shows the modulus of the frequency response of the closed-loop transfer function $\vec{I}_s(z)/\vec{I}_s^*(z)$, both for the mistuned plant.

The second condition to simulate will be a controller redesign, to test its performance when the resonance frequency

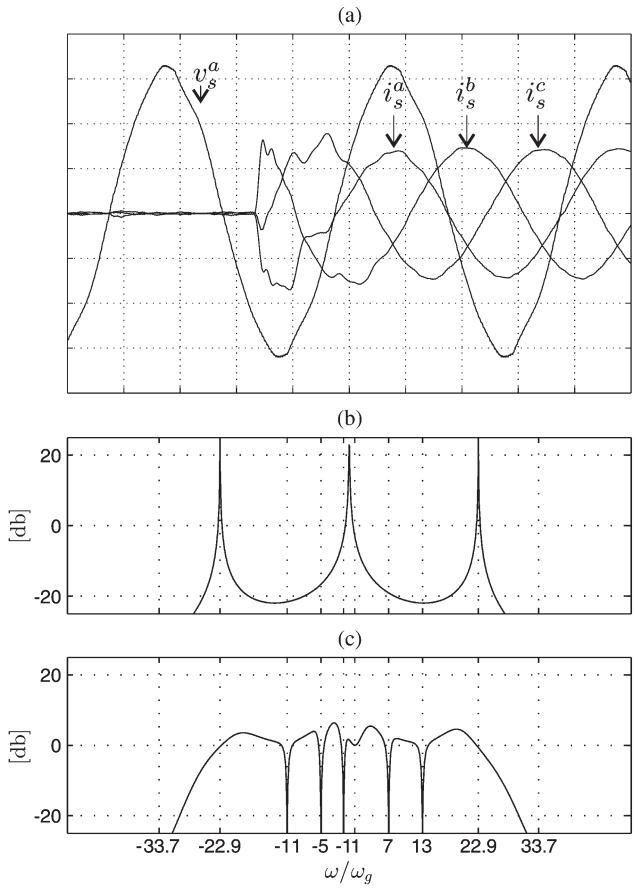

Fig. 11. (a) Simulated converter startup with parameter mismatch (voltage scale: 50 V/div, current scale: 5 A/div, time scale 5 ms/div). (b) Frequency response (modulus) of the open-loop LCL filter transfer function $\vec{I}_s(s)/\vec{V}_i(s)$. (c) Frequency response (modulus) of the closed-loop transfer function $\vec{I}_s(z)/\vec{I}_s(z)^*$.

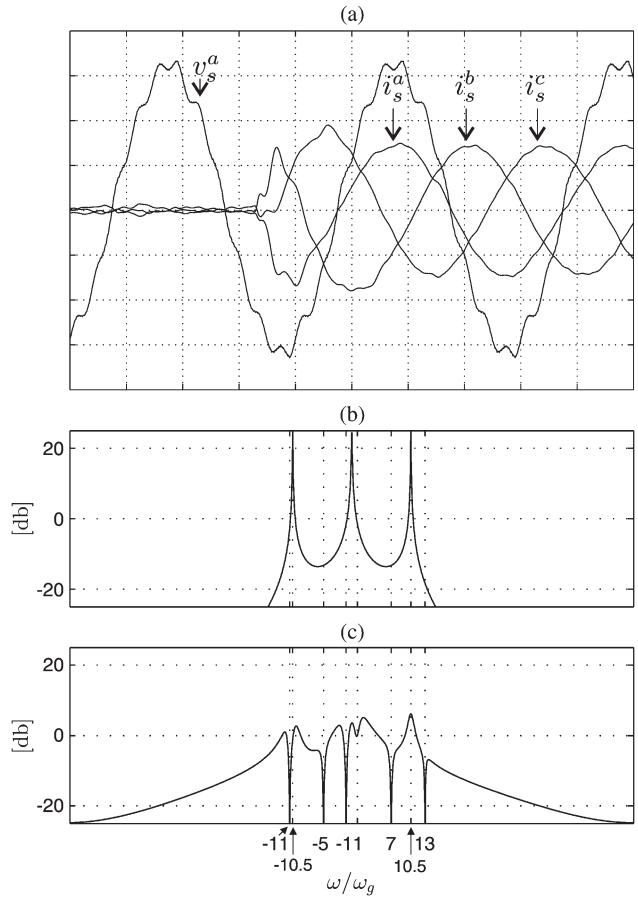

Fig. 12. (a) Simulated converter startup with LCL resonance at $10.5\omega_g$ (voltage scale: 50 V/div, current scale: 5 A/div, time scale 5 ms/div). (b) Frequency response (modulus) of the open-loop LCL filter transfer function $\vec{I}_s(s)/\vec{V}_i(s)$. (c) Frequency response (modulus) of the closed-loop transfer function $\vec{I}_s(z)/\vec{I}_s(z)^*$.

of the LCL filter is very low, which makes the AD challenging. The new resonance frequency was set close to the 11th harmonic of the grid voltage, at $10.5\ \omega_g$ (525 Hz). This allows us to also evaluate the behavior of the system when it is excited with a frequency close to the resonance of the filter. To do so, the nominal inductor values will be used ($L_1 = 1.5$ mH and $L_2 = 2.28$ mH), and the capacitor C will be increased 10.327 times its nominal value ($C = 102\ \mu$F). Note that the new resonance frequency is located below the poles of the current controller located at $+13\omega_g$ (650 Hz) and $-11\omega_g$ (550 Hz). The controller was then redesigned through the LQR method, choosing $Q = \text{diag}([1\ 1\ 1\ 1\ 1\ 1\ 1\ 1\ 1\ 1\ 1\ 1])$ and $R = 40$. Fig. 12(a) shows the grid voltage used for the test, which is contaminated with 5% of the 11th harmonic. Also, the time response of the new system is shown. As can be seen, this response is very similar to that obtained with the original LCL filter (see Fig. 8). In this case, the current had a THD $= 2.14\%$, whereas the grid voltage had a THD $= 5.74\%$. Fig. 12(b) and (c) shows the modulus of the frequency response of $\vec{I}_s(s)/\vec{V}_i(s)$ and $\vec{I}_s(z)/\vec{I}_s^*(z)$, respectively. These figures clearly show that the new resonance frequency is within the controller bandwidth.

VIII. Conclusion

It is concluded that a simple linear filter added to any linear current controller is all that is required for the AD of a grid-tie LCL inverter. Arbitrary assignment of all poles of the closed-loop system can be achieved with this filter. The proposed strategy allows the direct closed-loop control of the current injected to the grid, does not require more sensors than those needed to control a grid-tie L inverter, and adds low computational burden to that needed to control a grid-tie L inverter. A generalized design method for the current controller with AD has been presented, and it was verified that the closed-loop system is robust to parametric uncertainties. The experimental results obtained over a typical high-order current controller prove the feasibility of the proposal.

References

[1] P. Channegowda and V. John, "Filter optimization for grid interactive voltage source inverters," *IEEE Trans. Ind. Electron.*, vol. 57, no. 12, pp. 4106–4114, Dec. 2010.

[2] "*IEEE Standard for Interconnecting Distributed Resources With Electric Power Systems*," IEEE Std. 1547-2003, Sep. 2003.

[3] G. Shen, X. Zhu, J. Zhang, and D. Xu, "A new feedback method for PR current control of LCL-filter-based grid-connected inverter," *IEEE Trans. Ind. Electron.*, vol. 57, no. 6, pp. 2033–2041, Jun. 2010.

[4] M. Hanif, V. Khadkikar, W. Xiao, and J. Kirtley, "Two degrees of freedom active damping technique for LCL filter-based grid connected PV systems," *IEEE Trans. Ind. Electron.*, vol. 61, no. 6, pp. 2795–2803, Jun. 2014.
[5] M. Liserre, F. Blaabjerg, and S. Hansen, "Design and control of an LCL-filter-based three-phase active rectifier," *IEEE Trans. Ind. Appl.*, vol. 41, no. 5, pp. 1281–1291, Sep./Oct. 2005.
[6] R. Peña-Alzola *et al.*, "Analysis of the passive damping losses in LCL-filter-based grid converters," *IEEE Trans. Power Electron.*, vol. 28, no. 6, pp. 2642–2646, Jun. 2013.
[7] S.-Y. Park, C.-L. Chen, J.-S. Lai, and S.-R. Moon, "Admittance compensation in current loop control for a grid-tie LCL fuel cell inverter," *IEEE Trans. Power Electron.*, vol. 23, no. 4, pp. 1716–1723, Jul. 2008.
[8] F. Liu *et al.*, "Parameter design of a two-current-loop controller used in a grid-connected inverter system with LCL filter," *IEEE Trans. Ind. Electron.*, vol. 56, no. 11, pp. 4483–4491, Nov. 2009.
[9] Y. Tang *et al.*, "Generalized design of high performance shunt active power filter with output LCL filter," *IEEE Trans. Ind. Electron.*, vol. 59, no. 3, pp. 1443–1452, Mar. 2012.
[10] P. Dahono, "A control method to damp oscillation in the input LC filter," in *Proc. 33rd IEEE PESC*, 2002, vol. 4, pp. 1630–1635.
[11] Y. Tang, P. C. Loh, P. Wang, F. H. Choo, and F. Gao, "Exploring inherent damping characteristic of LCL-filters for three-phase grid-connected voltage source inverters," *IEEE Trans. Power Electron.*, vol. 27, no. 3, pp. 1433–1443, Mar. 2012.
[12] Y.-R. Mohamed, M. A-Rahman, and R. Seethapathy, "Robust line-voltage sensorless control and synchronization of LCL-filtered distributed generation inverters for high power quality grid connection," *IEEE Trans. Power Electron.*, vol. 27, no. 1, pp. 87–98, Jan. 2012.
[13] J. Dannehl, F. Fuchs, S. Hansen, and P. Thøgersen, "Investigation of active damping approaches for PI-based current control of grid-connected pulse width modulation converters with LCL filters," *IEEE Trans. Ind. Appl.*, vol. 46, no. 4, pp. 1509–1517, Jul./Aug. 2010.
[14] M. Malinowski and S. Bernet, "A simple voltage sensorless active damping scheme for three-phase PWM converters with an LCL filter," *IEEE Trans. Ind. Electron.*, vol. 55, no. 4, pp. 1876–1880, Apr. 2008.
[15] V. Blasko and V. Kaura, "A novel control to actively damp resonance in input LC filter of a three-phase voltage source converter," *IEEE Trans. Ind. Appl.*, vol. 33, no. 2, pp. 542–550, Mar./Apr. 1997.
[16] J. Xu, S. Xie, and T. Tang, "Active damping-based control for grid-connected LCL-filtered inverter with injected grid current feedback only," *IEEE Trans. Ind. Electron.*, vol. 61, no. 9, pp. 4746–4758, Sep. 2014.
[17] J. Yin, S. Duan, and B. Liu, "Stability analysis of grid-connected inverter with LCL filter adopting a digital single-loop controller with inherent damping characteristic," *IEEE Trans. Ind. Informat.*, vol. 9, no. 2, pp. 1104–1112, May 2013.
[18] R. Li, B. Liu, S. Duan, J. Yin, and X. Jiang, "Analysis of delay effects in single-loop controlled grid-connected inverter with LCL filter," in *Proc. 28th Annu. IEEE APEC*, Mar. 2013, pp. 329–333.
[19] S. Parker, B. McGrath, and D. Holmes, "Regions of active damping control for LCL filters," *IEEE Trans. Ind. Appl.*, vol. 50, no. 1, pp. 424–432, Jan./Feb. 2014.
[20] M. Liserre, A. Dell'Aquila, and F. Blaabjerg, "Stability improvements of an LCL-filter based three-phase active rectifier," in *Proc. 33rd IEEE PESC*, 2002, vol. 3, pp. 1195–1201.
[21] M. Liserre, A. Aquila, and F. Blaabjerg, "Genetic algorithm-based design of the active damping for an LCL-filter three-phase active rectifier," *IEEE Trans. Power Electron.*, vol. 19, no. 1, pp. 76–86, Jan. 2004.
[22] J. Dannehl, M. Liserre, and F. Fuchs, "Filter-based active damping of voltage source converters with LCL filter," *IEEE Trans. Ind. Electron.*, vol. 58, no. 8, pp. 3623–3633, Aug. 2011.
[23] R. Pena-Alzola *et al.*, "Systematic design of the lead–lag network method for active damping in LCL-filter based three phase converters," *IEEE Trans. Ind. Informat.*, vol. 10, no. 1, pp. 43–52, Feb. 2014.
[24] A. Reznik, M. Simoes, A. Al-Durra, and S. Muyeen, "LCL filter design and performance analysis for grid-interconnected systems," *IEEE Trans. Ind. Appl.*, vol. 50, no. 2, pp. 1225–1232, Mar./Apr. 2014.
[25] J. Dannehl, F. Fuchs, and P. Thogersen, "PI state space current control of grid-connected PWM converters with LCL filters," *IEEE Trans. Power Electron.*, vol. 25, no. 9, pp. 2320–2330, Sep. 2010.
[26] E. Wu and P. Lehn, "Digital current control of a voltage source converter with active damping of LCL resonance," *IEEE Trans. Power Electron.*, vol. 21, no. 5, pp. 1364–1373, Sep. 2006.
[27] X. Bao, F. Zhuo, Y. Tian, and P. Tan, "Simplified feedback linearization control of three-phase photovoltaic inverter with an LCL filter," *IEEE Trans. Power Electron.*, vol. 28, no. 6, pp. 2739–2752, Jun. 2013.
[28] J. Kukkola and M. Hinkkanen, "Observer-based state-space current control for a three-phase grid-connected converter equipped with an LCL filter," *IEEE Trans. Ind. Appl.*, vol. 50, no. 4, pp. 2700–2709, Jul./Aug. 2014.
[29] V. Miskovic, V. Blasko, T. Jahns, A. Smith, and C. Romenesko, "Observer-based active damping of LCL resonance in grid-connected voltage source converters," *IEEE Trans. Ind. Appl.*, vol. 50, no. 6, pp. 3977–3985, Nov./Dec. 2014.
[30] J. Kukkola, M. Hinkkanen, and K. Zenger, "Observer-based state-space current controller for a grid converter equipped with an LCL filter: Analytical method for direct discrete-time design in synchronous coordinates," in *Proc. IEEE ECCE*, Sep. 2014, pp. 4458–4465.
[31] P. Vas, *Electrical Machines and Drives: A Space-Vector Theory Approach*. Oxford, U.K.: Clarendon, 1992.
[32] R. Vaccaro, *Digital Control: A State Space Approach*. New York, NY, USA: McGraw-Hill, 1995.
[33] C. Busada, S. Gomez Jorge, A. Leon, and J. Solsona, "Current controller based on reduced order generalized integrators for distributed generation systems," *IEEE Trans. Ind. Electron.*, vol. 59, no. 7, pp. 2898–2909, Jul. 2012.
[34] W. Levine, *The Control Handbook, Second Edition (Electrical Engineering Handbook)*. Boca Raton, FL, USA: CRC Press, 2010.

Claudio A. Busada was born in Bahía Blanca, Argentina, on March 13, 1962. He received the degree in electrical engineering and the Dr. degree in control systems from the Universidad Nacional del Sur, Bahía Blanca, in 1989 and 2004, respectively.

From 1988 to 2004, he was with the Mechanical and Electrical Department, City of Bahía Blanca. Since 1989, he has been with the Departamento de Ingeniería Eléctrica y de Computadoras (DIEC), Universidad Nacional del Sur, where he is a Professor. He is a Researcher with the Instituto de Investigaciones en Ingeniería Eléctrica "Alfredo C. Desages" (UNS-CONICET). His research interests include power electronics, rotating machinery, active filters, automatic control, and integration of distributed energy systems.

Sebastian Gomez Jorge received the Electronics Engineer, M.S., and Dr. degrees from the Universidad Nacional del Sur, Bahía Blanca, Argentina, in 2006, 2009, and 2011, respectively.

He is currently with the Departamento de Ingeniería Eléctrica y de Computadoras, Instituto de Investigaciones en Ingeniería Eléctrica "Alfredo C. Desages" (IIIE), Universidad Nacional del Sur, where he is a Graduate Teaching Assistant, and with CONICET.

Jorge A. Solsona (SM'04) received the Electronics Engineer and Dr. degrees from the Universidad Nacional de La Plata, La Plata, Argentina, in 1986 and 1995, respectively.

He is currently with the Departamento de Ingeniería Eléctrica y de Computadoras, Instituto de Investigaciones en Ingeniería Eléctrica "Alfredo C. Desages" (IIIE), Universidad Nacional del Sur, Bahía Blanca, Argentina, where he is a Professor, and with CONICET. He is involved in teaching and research on control theory and its applications to electromechanical systems.